PERGAMON

International Journal of Solids and Structures 39 (2002) 1557–1573

INTERNATIONAL JOURNAL OF SOLIDS and STRUCTURES

www.elsevier.com/locate/ijsolstr

Numerical analysis of Biot's consolidation process by radial point interpolation method

J.G. Wang [a,*], G.R. Liu [b], P. Lin [c]

[a] *C/o Department of Civil Engineering, Tropical Marine Science Institute, National University of Singapore, 10 Kent Ridge Crescent, Singapore 119260, Singapore*

[b] *C/o Department of Mechanical Engineering, Centre of Advanced Computations in Engineering Science, National University of Singapore, 10 Kent Ridge Crescent, Singapore 119260, Singapore*

[c] *Department of Mathematics, National University of Singapore, 10 Kent Ridge Crescent, Singapore 119260, Singapore*

Received 22 February 2001; received in revised form 15 November 2001

Abstract

An algorithm is proposed to solve Biot's consolidation problem using meshless method called a radial point interpolation method (radial PIM). The radial PIM is advantageous over the meshless methods based on moving least-square (MLS) method in implementation of essential boundary condition and over the original PIM with polynomial basis in avoiding singularity when shape functions are constructed. Two variables in Biot's consolidation theory, displacement and excess pore water pressure, are spatially approximated by the same shape functions through the radial PIM technique. Fully implicit integration scheme is proposed in time domain to avoid spurious ripple effect. Some examples with structured and unstructured nodes are studied and compared with closed-form solution or finite element method solutions.

Keywords: Meshless method; Radial basis functions; Global equilibrium; Consolidation process; Pore water pressure

1. Introduction

Meshless methods have achieved remarkable progress in recent years. The diffuse element method (DEM) (Nayroles et al., 1992) was proposed earliest to use moving least-square (MLS) method to construct shape functions over a cluster of scattered nodes. Reproducing kernel particle method (Liu et al., 1995) introduced a correction function and a window function to improve the smoothed particle hydrodynamic method (SPH). Hp-cloud method (Duarte and Oden, 1996) was based on the partition of unity. Belytschko and his colleagues (Belytschko et al., 1994) improved the DEM based on Galerkin weak forms to form an element-free Galerkin (EFG) method. The EFG has been widely applied to various problems such as solid mechanics and deformable multiphase porous media (Modaressi and Aubert, 1998). Being different from above schemes, a novel interpolation scheme called point interpolation method (PIM) was proposed to

* Corresponding author. Tel.: +65-874-6591; fax: +65-779-1635.
E-mail address: tmswjg@nus.edu.sg (J.G. Wang).

0020-7683/02/$ - see front matter
PII: S0020-7683(02)00005-7

avoid the disadvantages of MLS (Liu and Gu, 2001; Wang et al., 2001). The shape functions obtained by PIM are of delta function properties. The original PIM (Liu and Gu, 2001) is based on polynomial basis functions. It works very well for one-dimensional (1D) problems because the rank of the polynomial is easily determined. When it is extended to multi-dimensional problems, the determination of the ranks is not an easy task. A major difficulty is to select basis functions. In order to overcome this difficulty, a radial PIM (Wang and Liu, 2001) was proposed. The basic idea was to map the multi-dimensional space into 1D space through a radial function. This mapping makes the choice of basis functions more easily. In order to include the accuracy of polynomials, the mixed bases of radial and polynomial bases are recommended in the radial PIM.

Radial basis functions have been successfully applied in partial differential equations (Kansa, 1990; Fasshauer, 1997; Wendland, 1999; Golberg et al., 1999; Coleman, 1996). Kansa (1990) was a pioneer who adopted radial basis functions to solve partial differential equations. He worked on the strong form and his algorithm was similar to the finite difference method (FDM). The difference is the method worked with both regular and irregular node distributions. Collocation methods with radial basis functions were recently developed as an effective meshless method (Fasshauer, 1997; Wendland, 1999; Zhang et al., 2000). Collocation methods are truly meshless methods. But they have two disadvantages except possibility of numerical stability: The first one is the difficulty to treat boundary conditions including internal and external boundaries. The current treatment is almost the same as the FDM. The second one is the requirement of higher order derivatives of shape functions. This requirement is sometimes difficult to be satisfied in practice, because higher smoothness will make the shape functions complicated. The meshless methods based on the weak form like Galerkin method are attractive to avoid above two demerits, although they require background mesh for integration. Because the background mesh is required, the meshless methods should be called pseudo-meshless methods.

This paper works on the meshless methods based on weak form. An algorithm for numerical solutions is proposed for the Biot's consolidation problem based on the radial PIM. This paper is organized as follows: Biot's consolidation theory is described through six physical concepts. This description can accommodate any constitutive law of materials and seepage although this paper treats only linear constitutive laws. Then its weak form is developed through a global equilibrium at each time step. Two spatial variables, displacement and excess pore pressure, are interpolated by the same shape functions constructed by radial PIM technique. A fully implicit scheme in time domain is suggested to avoid spurious ripple effect. Finally, 1D and two-dimensional (2D) consolidation problems are calculated and compared with closed-form solution or finite element (FEM) results available.

2. Biot's consolidation theory and its weak form

Soil skeleton and pore water consist of soil–water mixture of saturated soils. These two systems interact at micro-level. Biot's consolidation theory (Biot, 1941) provides a macro-level understanding for the interaction. It is composed of following six physical concepts:

- Equilibrium equation of soil–water mixture

$$\frac{\partial \sigma_{ij}}{\partial x_j} + b_i = 0 \quad \text{in } V \tag{1}$$

Or its incremental form in time interval $[t,\ t+\Delta t]$

$$\frac{\partial \Delta\sigma_{ij}}{\partial x_j} + \Delta b_i = -\left(\frac{\partial \sigma_{ij}^t}{\partial x_j} + b_i^t\right) \quad \text{in } V \tag{2}$$

- Relationship of displacement and strain for soil skeleton

$$\Delta\varepsilon_{ij} = \frac{1}{2}\left(\frac{\partial \Delta u_i}{\partial x_j} + \frac{\partial \Delta u_j}{\partial x_i}\right) \quad \text{in } V \tag{3}$$

- Constitutive law of soil skeleton in differential form

$$\mathrm{d}\sigma'_{ij} = D_{ijkl}\,\mathrm{d}\varepsilon_{kl} \quad \text{in } V \tag{4}$$

- Darcy's seepage law for pore water flow

$$q_i = \frac{K_{ij}}{\gamma_w}\frac{\partial P}{\partial x_j} \quad \text{in } V \tag{5}$$

- Terzaghi's effective stress principle

$$\sigma_{ij} = \sigma'_{ij} + P\delta_{ij} \tag{6}$$

- Continuity equation

$$\frac{\partial \varepsilon_v}{\partial t} = \frac{\partial q_i}{\partial x_i} \tag{7}$$

where σ_{ij}, σ'_{ij} and P are total stress tensor, effective stress tensor and excess pore water pressure at any time t and b_i the unit body force. Δu_i is the displacement increment and $\Delta\sigma_{ij}$, $\Delta\varepsilon_{ij}$ total stress and strain increments in time interval $[t, t+\Delta t]$. The discharge of excess pore water is q_i in ith direction. γ_w is the density of water. In SI system, its value can be taken as 10 kN/m^3. D_{ijkl} is the material matrix of soil skeleton determined by constitutive law of materials. K_{ij} is permeability tensor of soil skeleton which usually has non-zero components K_x in x direction and K_y in y direction, respectively. ε_v is the volume strain of soil skeleton:

$$\varepsilon_v = \frac{\partial u_i}{\partial x_i} \tag{8}$$

Boundary conditions include two parts: boundaries for solid and fluid

For soil skeleton boundary

$$\begin{cases} u_i = \bar{u}_{i0} & \text{on } S_{\bar{u}} \times [0,\infty) \\ \sigma'_{ij} n_j = \overline{T}_i & \text{on } S_\sigma \times [0,\infty) \end{cases} \tag{9}$$

Where $n = \{\, n_1 \quad n_2 \quad n_3 \,\}$ is the outwards normal direction and n_i is its directional cosine.

For fluid boundary

$$\begin{cases} P = P_0 & \text{on } S_p \times [0,\infty) \\ q_i = q_{i0} & \text{on } S_q \times [0,\infty) \end{cases} \tag{10}$$

Initial condition

$$\begin{cases} u_i = 0 \\ P = 0 \end{cases} \quad \text{on } V \times 0^- \tag{11}$$

If only soil skeleton is considered, it has two components of body forces:

(1) Effective unit weight $b'_i (= b_i - \gamma_w)$.
(2) Seepage force induced by hydraulic gradient $(-\partial P/\partial x_i)$.

In a time interval of $[t, t+\Delta t]$, displacement increments of soil skeleton should satisfy the weak form of equilibrium equation (2) of soil skeleton

$$\begin{aligned}&\int_V \{\delta(\Delta\varepsilon)\}^{\mathrm{T}}\{\Delta\sigma'\}\mathrm{d}v + \int_V \left\{\delta\left(\frac{\partial \Delta u_i}{\partial x_i}\right)\right\}^{\mathrm{T}}\{P\}^{t+\Delta t}\,\mathrm{d}v - \int_V \{\delta(\Delta\bar{\boldsymbol{u}})\}^{\mathrm{T}}\{\Delta b\}\mathrm{d}v \\ &\quad - \int_{S_\sigma}\{\delta(\Delta\bar{\boldsymbol{u}})\}^{\mathrm{T}}\{n\}P^{t+\Delta t}\,\mathrm{d}s - \int_{S_\sigma}\{\delta\left(\Delta\bar{\boldsymbol{u}}\right)\}^{\mathrm{T}}\{\Delta\overline{T}\}\,\mathrm{d}s \\ &= -\int_V \{\delta(\Delta\varepsilon)\}^{\mathrm{T}}\{\sigma''\}\,\mathrm{d}v + \int_{S_\sigma}\{\delta(\Delta\bar{\boldsymbol{u}})\}^{\mathrm{T}}\{\overline{T}\}^{t}\mathrm{d}v + \int_V \{\delta(\Delta\bar{\boldsymbol{u}})\}^{\mathrm{T}}\{b^t\}\,\mathrm{d}v\end{aligned} \tag{12}$$

where $\delta(\Delta\bar{\boldsymbol{u}})$ is the variational of displacement increment. The "δ" denotes the variational. The term at the right-hand side includes the un-balanced force at previous time step. This un-balanced force can be automatically corrected at the next step. Thus Eq. (12) can prevent error accumulation at each time step. It is possible to achieve the same accuracy at each time step. This auto-corrector is special useful in incremental computation schemes for dissipation problems.

Time integration is applied to continuity equation (7) and then the weak form for spatial variables (x, y) is expressed as

$$-\int_V \{\delta P\}^{\mathrm{T}}\left\{\frac{\partial \Delta u_i}{\partial x_i}\right\}\mathrm{d}v = -\frac{1}{\gamma_{\mathrm{w}}}\int_t^{t+\Delta t}\left[\int_{S_q}\{\delta P\}^{\mathrm{T}}\{q\}\,\mathrm{d}s\right]\mathrm{d}t + \frac{1}{\gamma_{\mathrm{w}}}\int_t^{t+\Delta t}\left[\int_V \left\{\frac{\partial \delta P}{\partial x_i}\right\}^{\mathrm{T}}\left\{K_i\frac{\partial P}{\partial x_i}\right\}\mathrm{d}v\right]\mathrm{d}t \tag{13}$$

where δP expresses the variational of displacement and excess pore water pressure in Eqs. (12) and (13), respectively.

Borja (1986) developed a finite element formulation for Biot's consolidation theory through a variational approach. His formulation is completely expressed in incremental form, not considering the accumulated errors at the previous time steps.

3. Radial point interpolation method

Consider an approximation function $u(\mathbf{x})$ in the influence domain. This function has a set of arbitrarily distributed points $P_i(\mathbf{x}_i)(i = 1, 2, \ldots, n)$ within the influence domain. n is the number of nodes. The function has value u_i at each node point $\mathbf{x}_i$. Radial PIM method constructs the $u(\mathbf{x})$ by passing through all these nodes. A general form is a linear combination of radial basis $B_i(\mathbf{x})$ and polynomial basis $p_j(\mathbf{x})$:

$$u(\mathbf{x}) = \sum_{i=1}^{n} B_i(\mathbf{x})a_i + \sum_{j=1}^{m} P_j(\mathbf{x})b_j = \mathbf{B}^{\mathrm{T}}(\mathbf{x})\mathbf{a} + \mathbf{P}^{\mathrm{T}}(\mathbf{x})\mathbf{b} \tag{14}$$

where a_i is the coefficient for $B_i(\mathbf{x})$ and b_j the coefficient for $p_i(\mathbf{x})$ (usually, $m < n$).

The vectors are defined as

$$\begin{aligned}&\mathbf{a}^{\mathrm{T}} = [\,a_1 \quad a_2 \quad a_3 \quad \cdots \quad a_n\,] \\ &\mathbf{b}^{\mathrm{T}} = [\,b_1 \quad b_2 \quad \cdots \quad b_m\,] \\ &\mathbf{B}^{\mathrm{T}}(\mathbf{x}) = [\,B_1(\mathbf{x}) \quad B_2(\mathbf{x}) \quad B_3(\mathbf{x}) \quad \cdots \quad B_n(\mathbf{x})\,] \\ &\mathbf{P}^{\mathrm{T}}(\mathbf{x}) = [\,p_1(\mathbf{x}) \quad p_2(\mathbf{x}) \quad \cdots \quad p_m(\mathbf{x})\,]\end{aligned} \tag{15}$$

Generally, the $B_i(\mathbf{x})$ has following form for a 2D problem

$$B_i(\mathbf{x}) = B_i(r_i) = B_i(x, y) \tag{16}$$

where r_i is the distance between interpolating point (x, y) and node (x_i, y_i) defined as

$$r_i = \left[(x - x_i)^2 + (y - y_i)^2\right]^{1/2} \tag{17}$$

Polynomial basis functions have following monomial terms:

$$\mathbf{P}^{\mathrm{T}}(\mathbf{x}) = \begin{bmatrix} 1 & x & y & x^2 & xy & y^2 & \cdots \end{bmatrix} \tag{18}$$

The coefficients a_i and b_j in Eq. (14) are determined by enforcing the $u(\mathbf{x})$ to pass through all n scattered points. For example, the interpolation at the kth point has

$$u_k = u(x_k, y_k) = \sum_{i=1}^{n} a_i B_i(x_k, y_k) + \sum_{j=1}^{m} b_j P_j(x_k, y_k) \quad k = 1, 2, \ldots, n \tag{19}$$

The polynomial term is an extra requirement. A constraint is necessary to insure that the approximation is unique:

$$\sum_{i=1}^{n} P_j(x_i, y_i) a_i = 0 \quad j = 1, 2, \ldots, m \tag{20}$$

It is expressed in matrix form as follows

$$\begin{bmatrix} \mathbf{B}_0 & \mathbf{P}_0 \\ \mathbf{P}_0^{\mathrm{T}} & \mathbf{0} \end{bmatrix} \begin{Bmatrix} \mathbf{a} \\ \mathbf{b} \end{Bmatrix} = \begin{Bmatrix} \mathbf{u}^{\mathrm{e}} \\ \mathbf{0} \end{Bmatrix} \quad \text{or} \quad \mathbf{G} \begin{Bmatrix} \mathbf{a} \\ \mathbf{b} \end{Bmatrix} = \begin{Bmatrix} \mathbf{u}^{\mathrm{e}} \\ \mathbf{0} \end{Bmatrix} \tag{21}$$

where the vector for function values at each node is

$$\mathbf{u}^{\mathrm{e}} = \begin{bmatrix} \mathrm{u}_1 & \mathrm{u}_2 & \mathrm{u}_3 & \cdots & \mathrm{u}_n \end{bmatrix}^{\mathrm{T}} \tag{22}$$

The coefficient matrix $\mathbf{B}_0$ on unknowns $\mathbf{a}$ is

$$\mathbf{B}_0 = \begin{bmatrix} B_1(x_1, y_1) & B_2(x_1, y_1) & \cdots & B_n(x_1, y_1) \\ B_1(x_2, y_2) & B_2(x_2, y_2) & \cdots & B_n(x_2, y_2) \\ \vdots & \vdots & \vdots & \vdots \\ B_1(x_n, y_n) & B_2(x_n, y_n) & \cdots & B_n(x_n, y_n) \end{bmatrix}_{n \times n} \tag{23}$$

The coefficient matrix $\mathbf{P}_0$ on unknowns $\mathbf{b}$ is

$$\mathbf{P}_0 = \begin{bmatrix} P_1(x_1, y_1) & P_2(x_1, y_1) & \cdots & P_m(x_1, y_1) \\ P_1(x_2, y_2) & P_2(x_2, y_2) & \cdots & P_m(x_2, y_2) \\ \vdots & \vdots & \vdots & \vdots \\ P_1(x_n, y_n) & P_2(x_n, y_n) & \cdots & P_m(x_n, y_n) \end{bmatrix}_{n \times m} \tag{24}$$

The distance is directionless, $B_k(x_i, y_i) = B_i(x_k, y_k)$. The unique solution is obtained if the inverse of matrix $\mathbf{G}$ or $\mathbf{B}_0$ exists:

$$\begin{Bmatrix} \mathbf{a} \\ \mathbf{b} \end{Bmatrix} = \mathbf{G}^{-1} \begin{Bmatrix} \mathbf{u}^{\mathrm{e}} \\ \mathbf{0} \end{Bmatrix} \tag{25}$$

The interpolation is finally expressed as

$$u(\mathbf{x}) = \left[\mathbf{B}^{\mathrm{T}}(\mathbf{x})\, \mathbf{P}^{\mathrm{T}}(\mathbf{x})\right] \mathbf{G}^{-1} \begin{Bmatrix} \mathbf{u}^{\mathrm{e}} \\ \mathbf{0} \end{Bmatrix} = \boldsymbol{\varphi}(\mathbf{x}) \mathbf{u}^{\mathrm{e}} \tag{26}$$

where the matrix of shape functions $\boldsymbol{\varphi}(\mathbf{x})$ is defined by

$$\begin{aligned}\boldsymbol{\varphi}(\mathbf{x}) &= [\,\phi_1(\mathbf{x}) \quad \phi_2(\mathbf{x}) \quad \cdots \quad \phi_i(\mathbf{x}) \quad \cdots \quad \phi_n(\mathbf{x})\,] \\ \phi_k(\mathbf{x}) &= \sum_{i=1}^{n} B_i(\mathbf{x})\overline{G}_{i,k} + \sum_{j=1}^{m} P_j(\mathbf{x})\overline{G}_{n+j,k}\end{aligned} \tag{27}$$

where $\overline{G}_{i,k}$ is the (i,k) element of matrix $\mathbf{G}^{-1}$. Once the inverse of matrix $\mathbf{G}$ is obtained, the derivatives of shape functions are

$$\begin{aligned}\frac{\partial \phi_k}{\partial x} &= \sum_{i=1}^{n} \frac{\partial B_i}{\partial x}\overline{G}_{i,k} + \sum_{j=1}^{m} \frac{\partial P_j}{\partial x}\overline{G}_{n+j,k} \\ \frac{\partial \phi_k}{\partial y} &= \sum_{i=1}^{n} \frac{\partial B_i}{\partial y}\overline{G}_{i,k} + \sum_{j=1}^{m} \frac{\partial P_j}{\partial y}\overline{G}_{n+j,k}\end{aligned} \tag{28}$$

Two particular forms of radial basis functions $B_i(x,y)$ are introduced hereafter: Multiquadrics and Gaussian type. Multiquadric basis (called MQ) was proposed by Hardy (1990). Its original form is extended to following form in this paper

$$B_i(x,y) = \left(r_i^2 + R^2\right)^q \quad R \geqslant 0 \tag{29}$$

where q and R are two parameters. The partial derivatives are obtained as follows

$$\begin{aligned}\frac{\partial B_i}{\partial x} &= 2q\left(r_i^2 + R^2\right)^{q-1}(x - x_i) \\ \frac{\partial B_i}{\partial y} &= 2q\left(r_i^2 + R^2\right)^{q-1}(y - y_i)\end{aligned} \tag{30}$$

Gaussian type (called EXP) radial functions are widely used in mathematics (Powell, 1992):

$$B_i(x,y) = \exp(-br_i^2) \tag{31}$$

where $b(b \geqslant 0)$ is a shape parameter. The partial derivatives are again obtained as follows

$$\begin{aligned}\frac{\partial B_i}{\partial x} &= -2bB_i(x,y)(x - x_i) \\ \frac{\partial B_i}{\partial y} &= -2bB_i(x,y)(y - y_i)\end{aligned} \tag{32}$$

4. Discretization of weak form

4.1. Spatial discretization

Displacement increment $(\Delta u_x, \Delta u_y)$ and excess pore water pressure P at any time t are discretized by the approximation given by Eq. (26). Eq. (12) is discretized as follows:

$$\mathbf{K}\Delta\mathbf{u} + \mathbf{K}_V\mathbf{P} = \Delta\mathbf{F}_\mathrm{b} + \Delta\mathbf{F}_\mathrm{t} + \mathbf{F}_\mathrm{r} \tag{33}$$

where $\mathbf{K}$ is the stiffness matrix of soil skeleton, $\mathbf{K}_V$ corresponds to the seepage force on the soil skeleton. The forces have three sources: body force increment $(\Delta\mathbf{F}_\mathrm{b})$, traction force increment $(\Delta\mathbf{F}_\mathrm{t})$ and residual force $(\mathbf{F}_\mathrm{r})$ due to un-equilibrium at the previous step. The vector $\Delta\mathbf{u}$ denotes for nodal displacement increments $\left(\Delta u_x, \Delta u_y\right)$ for all domain and vector $\mathbf{P}$ for the nodal excess pore pressure.

Similarly, Eq. (13) is discretized as follows:

$$\mathbf{K}_V^{\mathrm{T}}\Delta\mathbf{u} = \int_t^{t+\Delta t} \mathbf{K}_p\mathbf{P}\,\mathrm{d}t \tag{34}$$

As pointed out by Murad et al. (1996) and Murad and Loula (1994), different interpolations for displacement and pore water pressure will develop two kinds of methods: stable method whose displacement interpolation is one order higher than pore water pressure and unstable method whose interpolations are the same order for displacement and pore water pressure. They have different responses to the initial condition because the initial condition is the incompressible response of the solid–fluid aggregate.

4.2. Temporal discretization

Single step method is used in this paper. Any integrable function $f(x)$ is numerically integrated through following formula:

$$\int_t^{t+\Delta t} f(x)\,\mathrm{d}x = \Delta t[(1-\theta)f(t) + \theta f(t+\Delta t)] \tag{35}$$

Here $0 \leqslant \theta \leqslant 1$. Combining Eqs. (33)–(35) obtains

$$\begin{bmatrix} \mathbf{K} & \mathbf{K}_V \\ \mathbf{K}_V^{\mathrm{T}} & -\Delta t\,\theta\mathbf{K}_p \end{bmatrix} \begin{Bmatrix} \Delta\mathbf{u} \\ \mathbf{P} \end{Bmatrix} = \begin{Bmatrix} \Delta\mathbf{F}_{\mathrm{b}} + \Delta\mathbf{F}_{\mathrm{t}} + \mathbf{F}_{\mathrm{r}} \\ \Delta t(1-\theta)\mathbf{K}_p\mathbf{P}^t \end{Bmatrix} \tag{36}$$

The value of θ is important to accuracy, stability and spurious ripple effect. The analysis has shown that the condition for no spurious ripple effect is as follows:

$$\zeta\Delta t < \frac{1}{1-\theta} \tag{37}$$

where ζ is an eigenvalue. Hence for any value of $\theta \neq 1$ the numerical solution can exhibit a spurious ripple effect for values which are not satisfied with Eq. (37). The approximation is unconditionally stable when $\theta \geqslant 0.5$. $\theta = 0$ is fully explicit Euler algorithm that is stable only when time step size is small enough (Wood, 1990). The time step size is also imposed from the condition of no spurious ripple effect as expressed by Eq. (37). $\theta = 1$ is fully implicit (backward Euler) algorithm. There is no requirement on time step size from both stability and spurious ripple effect. The algorithm has the unique second order accuracy only when $\theta = 0.5$, which is the famous Crank–Nicolson (1949) scheme. Fully implicit algorithm is recommended in this paper. When $\theta = 1$, Eq. (36) becomes

$$\begin{bmatrix} \mathbf{K} & \mathbf{K}_V \\ \mathbf{K}_V^{\mathrm{T}} & -\Delta t\mathbf{K}_p \end{bmatrix} \begin{Bmatrix} \Delta\mathbf{u} \\ \mathbf{P} \end{Bmatrix} = \begin{Bmatrix} \Delta\mathbf{F}_{\mathrm{b}} + \Delta\mathbf{F}_{\mathrm{t}} + \mathbf{F}_{\mathrm{r}} \\ 0 \end{Bmatrix} \tag{38}$$

This is to say that the excess pore water pressure at the previous step has no contribution to the current load vector.

5. Assessment through numerical examples

5.1. One-dimensional consolidation problem

A regular node distribution is shown in Fig. 1 (833 nodes). Single-side drainage is assumed. Two sides and bottom are all fixed for displacements. Thickness of the soil layer is assumed to be $H = 16$ m. Soil parameters are assumed as linear elasticity with $E = 40000$ kPa, $v = 0.3$ and $k = 1.728 \times 10^{-3}$ m/day.

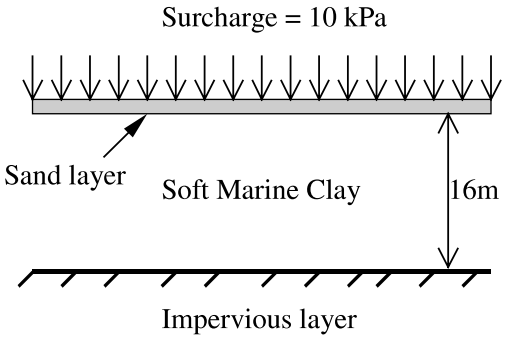

(a) Physical model for 1D consolidation problem

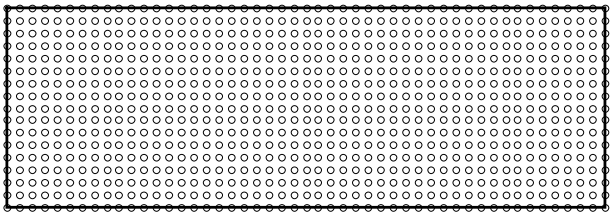

(b) Node distributions for meshless methods

Fig. 1. 1D Terzaghi's consolidation problem and meshless model.

Surcharge at the upper surface is $\Delta\sigma = 10$ kPa. Closed-form solution for this problem (Terzaghi and Peck, 1976) is:

$$P = \frac{4}{\pi}\Delta\sigma \sum_{n=1}^{\infty} \frac{1}{2n-1} \sin\left(\frac{(2n-1)\pi y}{2H}\right) e^{-(2n-1)^2 \frac{\pi^2}{4} T_V} \tag{39}$$

Degree of consolidation U_t is

$$U_t = 1 - \frac{8}{\pi^2} \sum_{n=1}^{\infty} \frac{1}{(2n-1)^2} e^{-(2n-1)^2 \frac{\pi^2}{4} T_V} \tag{40}$$

where the parameters are defined as

$$T_V = \frac{C_V}{H^2} t, \quad C_V = \frac{k}{\gamma_w m_v}, \quad m_v = \frac{(1+v)(1-2v)}{E(1-v)} \tag{41}$$

Surface settlement S_t at any time t is given by

$$S_t = U_t m_v \Delta\sigma H \tag{42}$$

The regular node distribution is used for comparison. Influence domain is taken as 1.5 and average nodes in each Gauss point are 15.34. The EXP basis function with parameter $b = 0.025$ is used. Linear polynomial ($m = 3$) is also included for all following cases. Time domain uses fully implicit scheme for discretization. Two time step sizes are designed to adapt different dissipation rates. Time step size is 0.2 days before 2 days and 1.2 days within the subsequent 18 days. Numerical results are compared with the closed-form solution above. Fig. 2 compared the surface settlement of the layer and Fig. 3 compared the dissipation process of excess pore water pressure at three node points. They agree well with closed-form solutions. The excess pore water pressures are almost the same within the layer at the beginning of consolidation. They dissipate

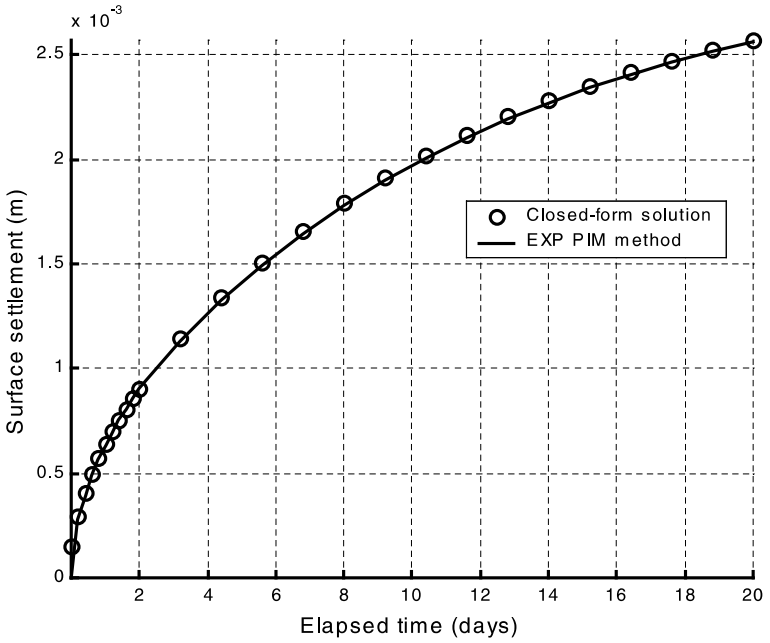

Fig. 2. Surface settlement curve and comparison with closed-form solution.

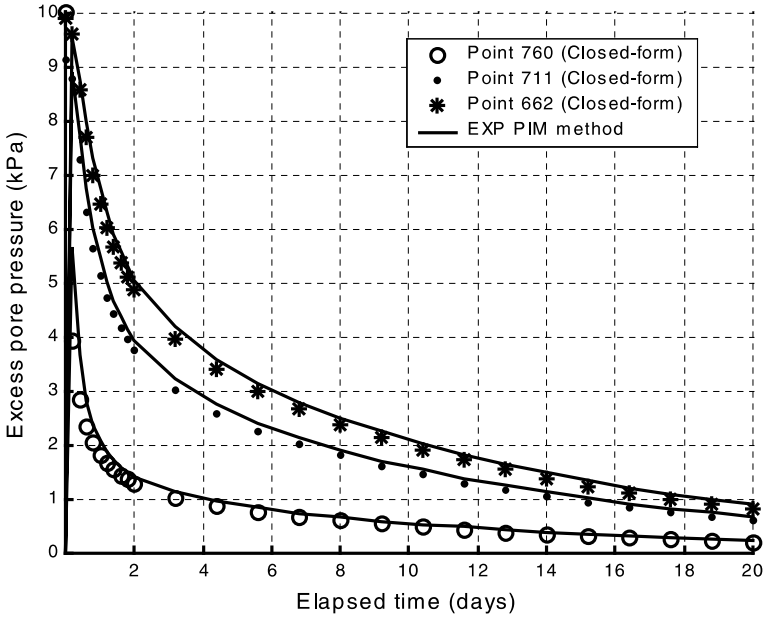

Fig. 3. Dissipation of excess pore water pressure at different points (compared with closed-form solution).

quickly in the first three days and then dissipate gradually. The dissipation is almost completed after 20 days. This is due to the high permeability of soil layer.

5.2. Two-dimensional consolidation problem under strip foundation

A 2D problem of consolidation is presented here. A schematic model and its meshless models are shown in Fig. 4. This is a plane strain consolidation problem under a strip loading of 10 kPa. Foundation soil is the same as 1D case. Top surface is full drainage and the rest boundaries are all impervious. Horizontal displacement is fixed along vertical boundary and vertical displacement is fixed along horizontal boundary. EXP basis with linear polynomial is used. There is no closed-form solution available, thus FEM is carried out for comparison. The FEM uses four-node isoparametric elements with the same (regular) nodes as meshless methods. All other conditions are the same as meshless methods. Initial values for displacement and excess pore water pressure are given zeros as pointed out by Eq. (11), but these are the values at the time 0^-. The values at the time 0^+ are obtained through giving short time step size ($\Delta t = 0.001$ day in this example) and letting the drainage boundary all un-drainage. This can approximately simulate the un-drainage conditions (Borja, 1986; Murad et al., 1996). After initial values at time 0^+ are obtained, subsequent time steps are carried out through Eq. (38).

The numerical results for regular node distribution are presented here. Fig. 5 shows the dissipation history of excess pore water pressure along the middle line of the foundation. The FEM results are also plotted for comparison. Generally, both agree very well. Again, the dissipation process is faster within three days. When time elapses about 20 days, dissipation process of excess pore water pressure almost completes.

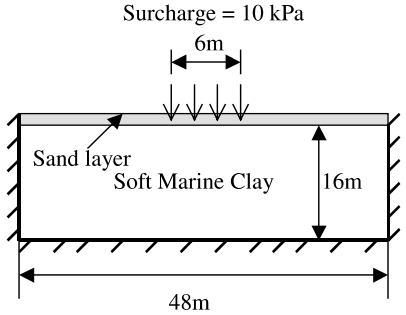

(a) 2D consolidation problem under strip load

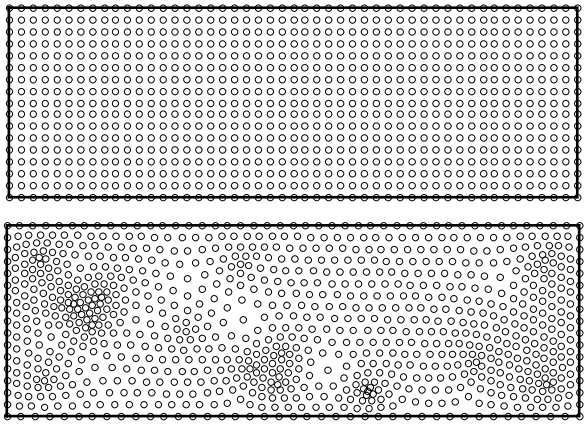

(b) Meshless models for 2D problem (regular and irregular nodes)

Fig. 4. 2D consolidation problem under strip load.

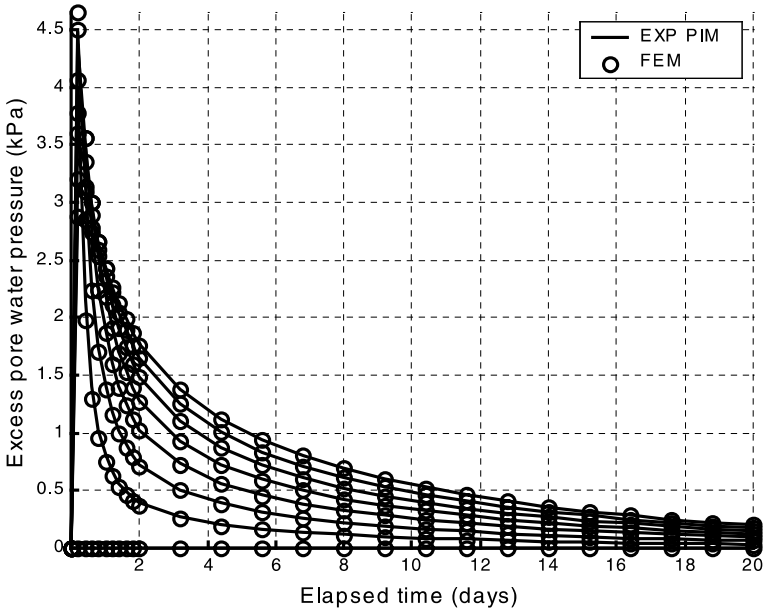

Fig. 5. Dissipation of excess pore water pressure along middle line.

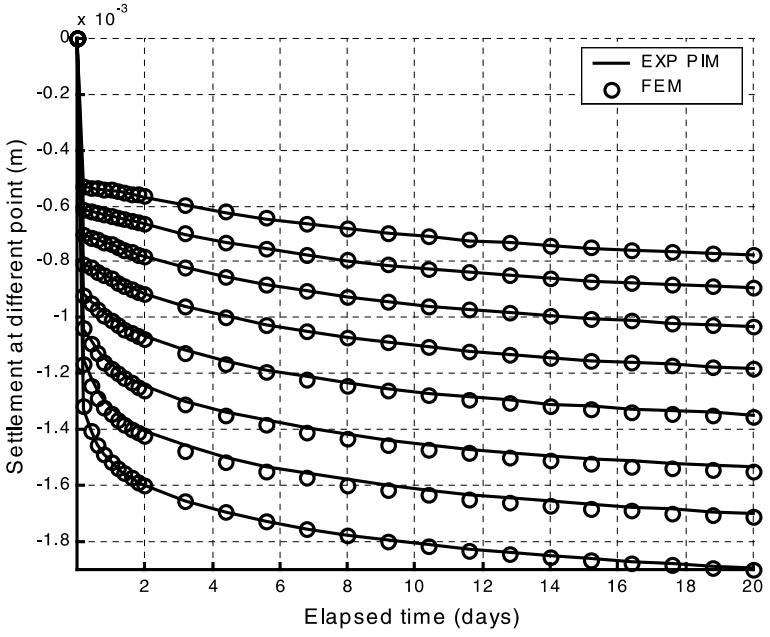

Fig. 6. Displacement distribution along middle line.

Correspondingly, the vertical displacements, u_y, reach their stable states as shown in Fig. 6. Foundation has an immediate displacement after surface load although no pore water pressure dissipates. This displacement corresponds to the elastic deformation of soil–water mixture without volume change and has no time effect.

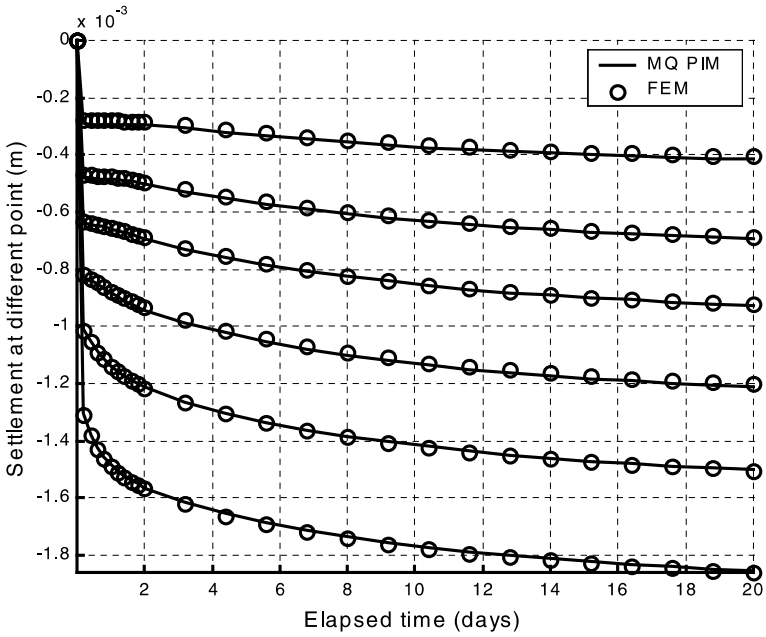

Fig. 7. Comparison of displacements for node irregularity.

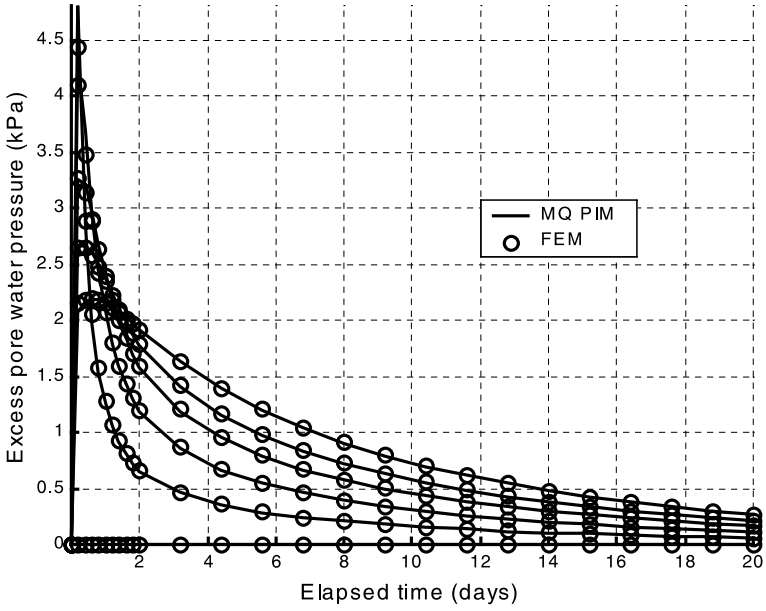

Fig. 8. Comparison of dissipation process for node irregularity.

Biot's consolidation theory treats dissipation of pore water pressure and deformation of soil skeleton simultaneously, thus the deformation and the dissipation are obtained at the same time. The displacement

is subsequently increasing with the dissipation of excess pore water pressure and finally reaches its stable value when dissipation process stops.

Unstructured or irregular node distribution (915 nodes) as shown in Fig. 4 is used here to check the suitability of the radial PIM. Influence domain is the same as above. Average node points per Gaussian

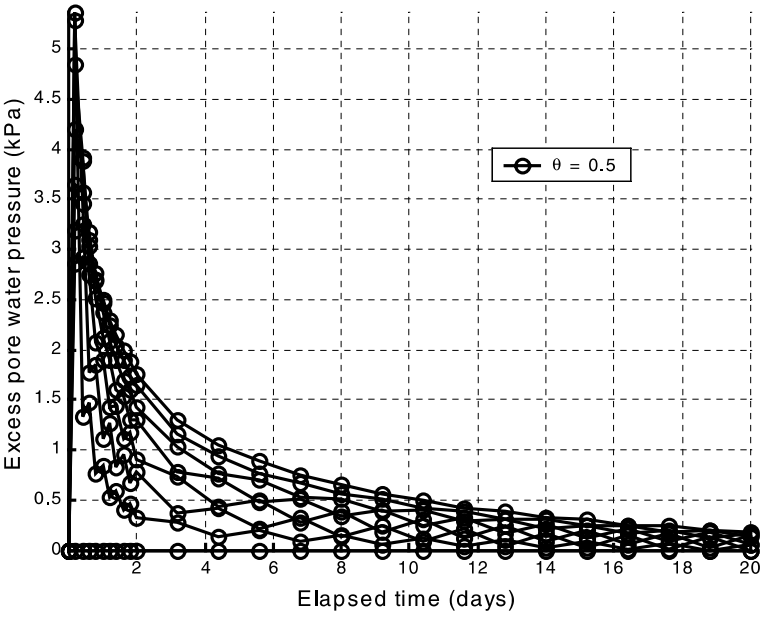

(a) Spurious ripple effect in 2D problem

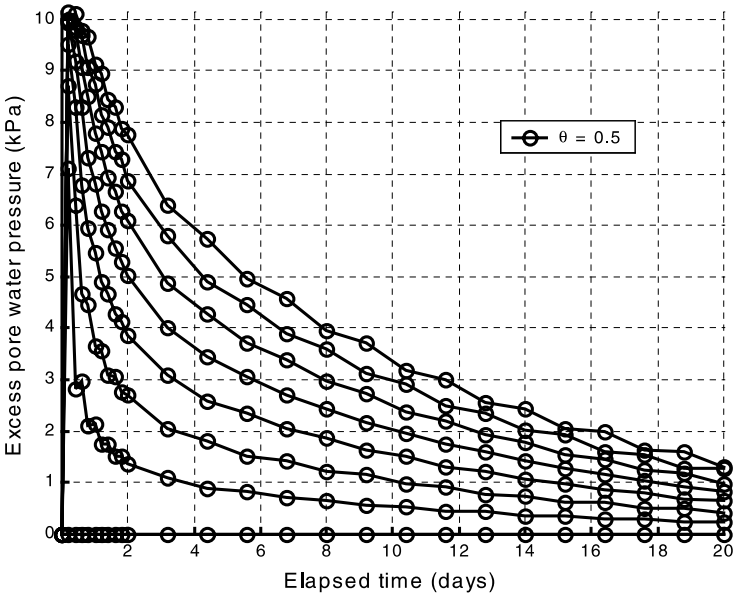

(b) Spurious ripple effect in Terzaghi problem

Fig. 9. Spurious ripple effect when $\theta = 0.5$.

point are 10.72 and the maximum number of nodes is limited to 30. MQ method ($q = 1.03, R = 0.1$) is used in the computation. Fig. 7 compared the settlement and Fig. 8 compared the dissipation of excess pore water pressure at different node points. They show that the radial PIM method is not sensitive to the irregularity of node distribution. Both regular and irregular node distributions give satisfactory results. As a conclusion from above two examples, the radial PIM method is feasible in solving Biot's consolidation problems whether the node distribution is structured or unstructured.

5.3. Time integration factor θ

Spurious ripple effect is observed when time integration factor is taken as $\theta = 0.5$. The time step size here is the same as fully implicit scheme. Although Crank–Nicolson scheme has second order of accuracy, the spurious ripple effect will affect numerical stability. Fully implicit scheme is only one order of accuracy, but no spurious ripple effect is observed. This is its advantage. Fig. 9 gives a typical dissipation curve along middle line for 1D and 2D problems when $\theta = 0.5$. Obviously, Crank–Nicolson scheme has spurious ripple effect for both problems under current time step sizes. It is noted that the spurious ripple stems from drainage boundaries and dissipates into internal nodes as shown in Fig. 9(b). The higher order accuracy is lost due to this spurious ripple effect. From the view of computation, the Crank–Nicolson scheme spends more CPU time on converting the previous node pressure into current node load as given by Eq. (36). Therefore, fully implicit scheme is a better choice for numerical computation.

5.4. Effect of radial basis functions

This section compares the numerical results obtained through MQ and EXP basis functions. Fully implicit scheme is used for time domain ($\theta = 1.0$). The model parameters are $q = 1.03$ and $R = 0.1$ for MQ basis and $b = 0.025$ for EXP basis. Regular and irregular node distributions are used for both 1D and 2D problems. Fig. 10 shows typical curves of excess pore water pressure and vertical displacement for the 2D problem under regular node distribution. Fig. 11 compares the numerical results obtained from irregular node distribution. Basically, the results agree well for different radial basis functions. Therefore, the radial PIM with EXP and MQ bases is suitable for any node distribution. Our computations also indicate that MQ basis is more numerical stable and has higher accuracy than EXP basis if the constant influence domain size is applied to the whole problem domain.

6. Conclusions

The radial PIM with linear polynomials is applied to study the numerical solution of Biot's consolidation problem in foundation engineering. We first study the expression of the Biot's theory for general constitutive laws of soil skeleton. A weak form for error auto-corrector is developed based on this expression. Spatial variables of displacement increment and excess pore water pressure are all discretized by the same radial PIM shape function. Time domain is discretized by fully implicit scheme to eliminate spurious ripple effect. Some examples demonstrate its feasibility and effectiveness. From these studies, following conclusions can be drawn:

First, radial PIM is an effective interpolation technique for scattered node distributions. It is suitable not only for structured nodes but also for unstructured nodes without any singularity problem. This is its advantage over the original PIM with only polynomial basis. Unlike meshless methods based on the MIS method, the radial PIM method obtains its shape function and derivatives once $\mathbf{B}_0^{-1}$ or $\mathbf{G}^{-1}$ is obtained and shape functions are of delta function properties, thus essential boundary conditions are easily implemented.

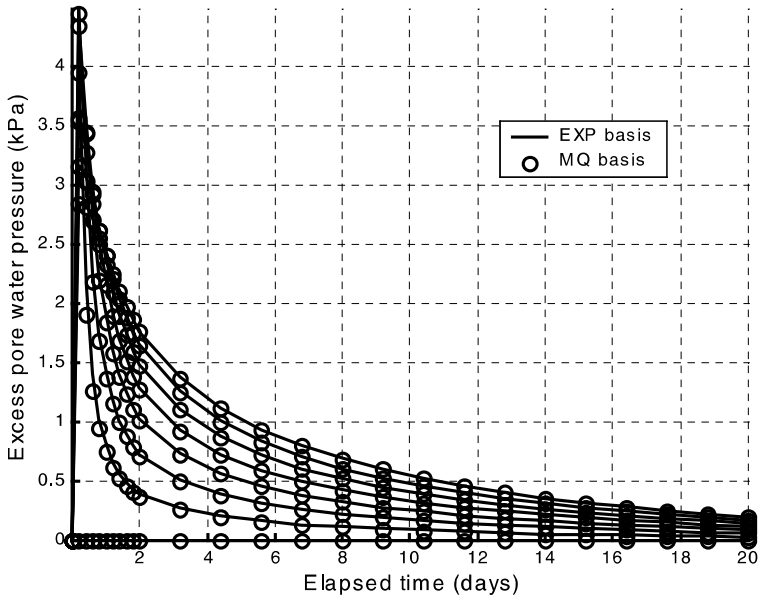

(a) Comparison of excess pore water pressure by EXP and MQ bases

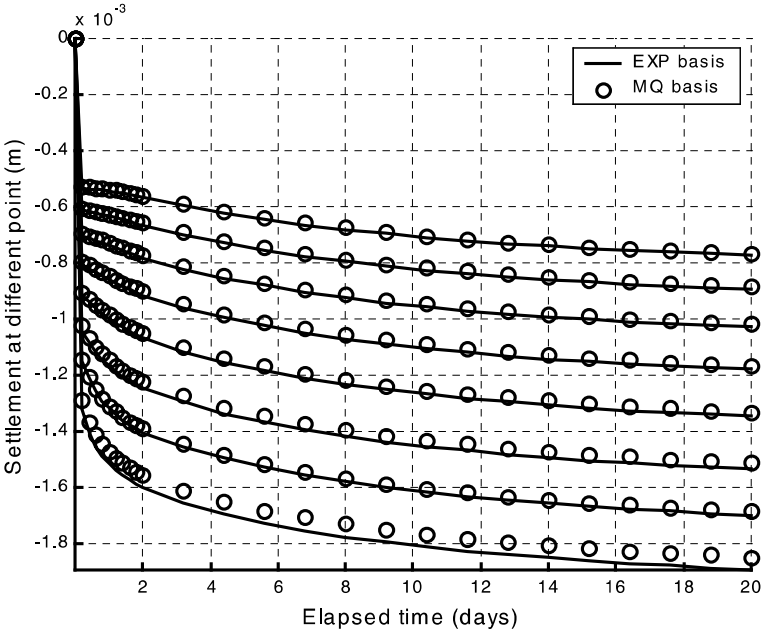

(b) Comparison of displacement by EXP and MQ bases

Fig. 10. Numerical results of 2D problem obtained by EXP and MQ bases (over regular node distribution).

Second, both EXP basis and MQ basis have good accuracy for any node distribution. The examples show that the MQ basis is more stable than EXP basis for unstructured and variable density node distribution. The choice of model parameters will affect the accuracy of radial PIM. The $b = 0.025$ for EXP

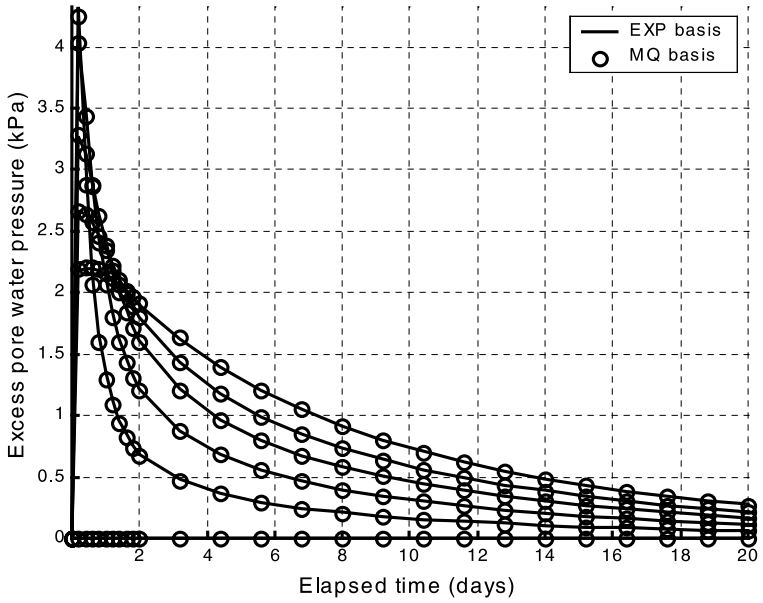

(a) Comparison of excess pore water pressure

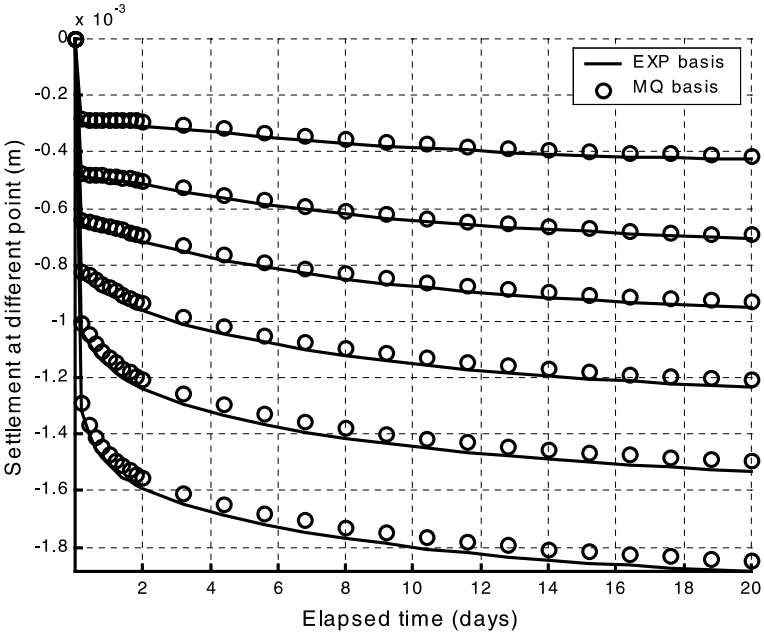

(b) Comparison of displacement

Fig. 11. Numerical results of 2D problem over irregular node distribution.

basis and $q = 1.03$, $R = 0.1$ for MQ basis are good parameters for the examples in this paper. Parameter study is a complicated problem that will be discussed in another paper.

Third, spurious ripple effect can be avoided if proper time discretization scheme is used, even if the same shape functions are used for both displacement and excess pore water pressure. Fully implicit scheme in this paper is free of spurious ripple scheme, while Crank–Nicolson scheme requires time step size within some range. Therefore, the time step size in fully implicit scheme can be bigger than Crank–Nicolson scheme.

Finally, the weak form developed in this paper is suitable for radial meshless method. This weak form can automatically correct the error during each time step and thus keep the same accuracy of global balance. This correction prevents the propagation of numerical error with time step. On this meaning, the weak form is useful not only for the numerical solution of Biot's consolidation problems but also for non-linear problems.

References

Belytschko, T., Lu, Y.Y., Gu, L., 1994. Element-free Galerkin methods. Int. J. Numer. Meth. Engng. 37, 229–256.

Biot, M.A., 1941. General theory of three-dimensional consolidation. J. Appl. Phys. 12, 155–164.

Borja, R., 1986. Finite element formulation for transient pore pressure dissipation: A variational approach. Int. J. Solids Struct. 22, (11), 1201–1211.

Coleman, C.J., 1996. On the use of radial basis functions in the solution of elliptic boundary value problems. Comput. Mech. 17, 418–422.

Crank, J., Nicolson, P., 1949. A practical method for the numerical integration of solutions of partial differential equations of heat conduction type. Proceedings of the Cambridge Philosophical Society 43, 50–67.

Duarte, C.A., Oden, J.T., 1996. Hp clouds—an h–p meshless method. Numer. Meth. Partial Different. Equat. 12, 673–705.

Fasshauer, G.E., 1997. Solving partial differential equations by collocation with radial basis functions. In: Mehaute, A.L., Rabut, C., Schumaker, L.L. (Eds.), Surface Fitting and Multiresolution Methods, Nashville, TN: Vanderbilt University Press, 1997. pp. 131–138.

Golberg, M.A., Chen, C.S., Bowman, H., 1999. Some recent results and proposals for the use of radial basis functions in the BEM. Engng. Anal. Boundary Elements 23, 285–296.

Hardy, R.L., 1990. Theory and applications of the multiquadrics—Biharmonic method (20 years of discovery 1968–1988). Comput. Math. Appl. 19, 163–208.

Kansa, E.J., 1990. A scattered data approximation scheme with application to computational fluid-dynamics—I & II. Comput. Math. Appl. 19, 127–161.

Liu, G.R., Gu, Y.T., 2001. A point interpolation method for two-dimensional solids. Int. J. Numer. Meth. Engng. 50, 937–951.

Liu, W.K., Jun, S., Zhang, Y.F., 1995. Reproducing kernel particle methods. Int. J. Numer. Meth. Fluids 20, 1081–1106.

Modaressi, H., Aubert, P., 1998. Element-free Galerkin method for deforming multiphase porous media. Int. J. Numer. Meth. Engng. 42, 313–340.

Murad, M.A., Thomee, V., Loula, A.F.D., 1996. Asymptotic behaviour of semidiscrete finite element approximations of Biot's consolidation problems. SIAM J. Numer. Anal. 33 (3), 1065–1083.

Murad, M.A., Loula, A.F.D., 1994. On stability and convergence of finite element approximations of Biot's consolidation problems. Int. J. Numer. Meth. Engng. 37, 645–667.

Nayroles, B., Touzot, G., Villon, P., 1992. Generalizing the finite element method: diffuse approximation and diffuse elements. Comput. Mech. 10, 307–318.

Powell, M.J.D., 1992. The theory of radial basis function approximation in 1990. In: Light, F.W. (Ed.), Advances in Numerical Analysis, Oxford University Press. pp. 105–203.

Terzaghi, K., Peck, R.B., 1976. Soil Mechanics in Engineering Practice, second ed. John Wiley & Sons Inc., New York.

Wang, J.G., Liu, G.R., 2001. A point interpolation meshless method based on radial basis functions. Int. J. Numer. Meth. Engng., in press.

Wang, J.G., Liu, G.R., Wu, Y.G., 2001. A point interpolation method for simulating dissipation process of consolidation. Comput. Meth. Appl. Mech. Engng. 190 (45), 5907–5922.

Wendland, H., 1999. Meshless Galerkin method using radial basis functions. Math. Comput. 68 (228), 1521–1531.

Wood, W.L., 1990. Practice Time-stepping Schemes. Clarendon Press, Oxford.

Zhang, X., Song, K.Z., Lu, M.W., 2000. Meshless methods based on collocation with radial basis functions. Comput. Mech. 26 (4), 333–343.